18TH WORLD CONFERENCE ON EARTHQUAKE ENGINEERING
WCEE2024
MILAN
MILAN, ITALY
30TH JUNE - 5TH JULY 2024
www.wcee2024.it

# 30 YEARS OF DIRECT DISPLACEMENT-BASED DESIGN: WHERE WE STARTED, WHAT'S BEEN DONE, WHERE WE'RE GOING

M. J. Kowalsky[1] & A. L. Palma Parra[2]

[1]North Carolina State University, Raleigh, NC, United States of America, kowalsky@ncsu.edu

[2]North Carolina State University, Raleigh, NC, United States of America

**Abstract**: *In 1993, Nigel Priestley drafted the outline for what would become Direct Displacement-Based Design (DDBD) in his paper titled "Myths and fallacies in Earthquake Engineering: Conflicts between design and reality." Shortly after, the methodology was developed for SDOF systems, and then for more complex bridges and buildings. The procedure was subjected to extensive verification, including non-linear time history analysis. In this paper, the origin story and advances in DDBD are described. Discussed is the impact of bi-directional response on systems, including simplifications for considerations of different response spectra definitions. The paper continues by proposing a simplification to DDBD that addresses the sensitivity of damping values and hysteretic shapes on required strength. This results in a simplified version of the approach whereby a system may be designed assuming a single target ductility and hysteretic response, and the resulting outcome adjusted based on system type and target displacement. Discussed next are further challenges currently under investigation, including the a priori definition of a system displaced shape, the advent of multi-point spectra, and directionality for complex systems such as multi-span bridges. It is the hope that this paper will encourage continued development and implementation of DDBD around the world.*

## 1. Introduction

The origin of Direct Displacement-Based Seismic Design (DDBD) can be traced to the paper "Myths and fallacies in Earthquake Engineering: Conflicts between design and reality" (Priestley, 1993). Some early hand sketches of the fundamentals of the approach are shown in Figure 1, which were from a meeting at the start of the first author's graduate studies at UCSD in 1993. This sketch illustrates all the essential elements of the approach as originally envisioned by Priestley. Namely, given a demand, expressed in the form of a displacement response spectrum, a single-degree-of-freedom (SDOF) system is designed to achieve a target displacement by entering the spectra with that displacement and reading across to the appropriately damped spectra to determine the effective period of the structure. The relationship between damping and ductility, which has been an active area of research over the last 20 years, is qualitatively shown for different hysteretic systems. Finally, the effective stiffness of the structure is obtained from the effective period, and the base shear obtained by multiplying that stiffness by the target displacement. All of these steps, which are well understood and established in 2023, can be seen in this 1993 hand sketch (Figure 1). By assuming a displacement response spectrum that is linear to the corner point, the DDBD base shear can be calculated via Equation 1. The procedure has been extended to multi-degree-of-freedom (MDOF) systems as explained in Priestley et al. (2007). Furthermore, extensive verification for a variety of systems has shown that structures designed with DDBD achieve their target displacement when subjected to nonlinear time history analysis (NTHA) with ground motions that are compatible with the design spectra. Examples of such verifications are shown in Figure 2 (Dwairi et al., 2006), which illustrates the target displacement that a series of bridges have been designed for, along with the results of nonlinear time history analysis using spectrum compatible records. Note that the time history analysis results align well with the target displacement pattern, demonstrating the procedure's capability to define a target performance level that the resulting structure will achieve when subjected to ground motion consistent with its design.

$$V_{Base} = K_e \cdot \Delta_d = \frac{4\pi^2 m_e}{T_c^2} \cdot \frac{\Delta_{c,5}^2}{\Delta_d} \cdot \frac{7}{2+\xi} \quad (1)$$

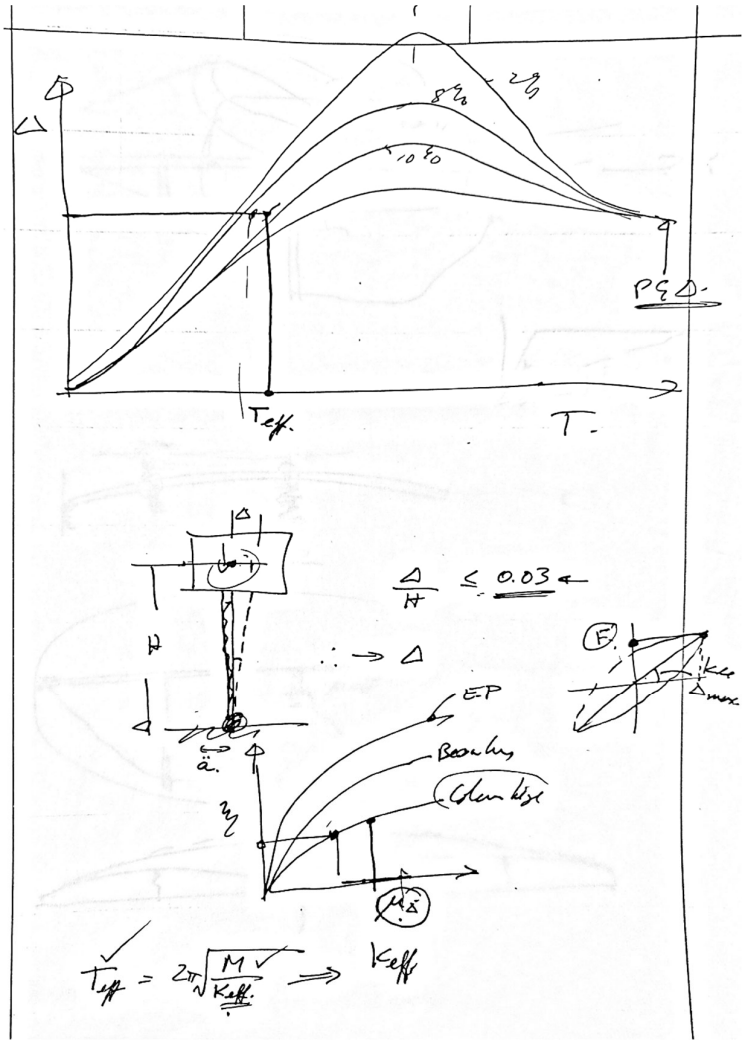


*Figure 1. Initial sketch of Direct Displacement-Based Design approach by Priestley*

In the following sections of this paper, we delve into potential avenues to simplify DDBD approach without reducing accuracy. First, we focus on the application of the DDBD approach under bidirectional loading and simplifications to account for directionality definitions of the design spectra. Second, we propose and demonstrate a simplified procedure that accounts for equivalent viscous damping in DDBD for different hysteretic systems. While the calculation of damping within the current approach is well defined, it can be an iterative process.

Furthermore, an extension of this approach into MDOF systems, such as multi-span bridges, has been addressed by Priestley et al. (2007) and is proposed in the upcoming AASHTO performance-based design guidelines as an alternative bridge design approach (AASHTO, 2023). It is worth noting that DDBD, especially when applied to bridge structures, requires some iteration to converge onto a displaced shape. These issues are also addressed within the scope of this paper. It is the hope that this paper provides a historical summary of the development of DDBD while also indicating some future directions to facilitate broader implementation.

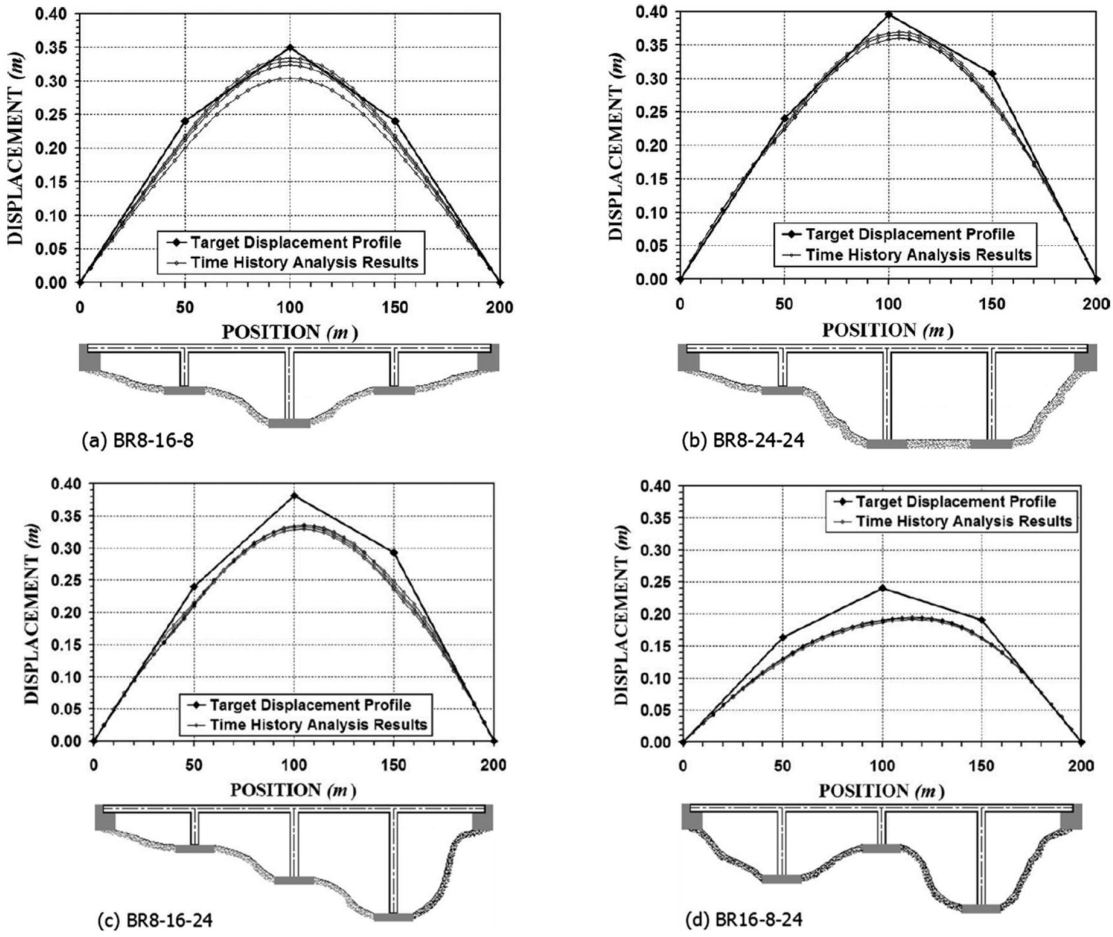


*Figure 2. Maximum transverse displacements from nonlinear analyses compared to target displacement profile given by DDBD. Bridges designed with abutment restrained in the transverse direction with rotation allowed (Modified from Dwairi et al, 2006).*

## 2. Bidirectional response spectra and DDBD

Until the master's studies of the second author, all studies (to the knowledge of the authors) on DDBD were conducted using single direction seismic attack. However, it is well established that ground motion records are comprised of the recorded signals in the three orthogonal directions. While there are exceptions that depend on factors such as site conditions, the accelerations in the horizontal plane have historically caused more damage to structures than accelerations in the vertical plane, for which the amplitude is usually lower. Due to this, response spectra are typically computed based only on the two horizontal components of ground motion records. Moreover, to capture the possible demands in any direction, design spectra have used various measures to define this ground motion directionality, such as the RotDnn measure where "nn" is the percentile of the peak response across all possible orientations of the ground motion, making it independent of the in-situ sensor orientation (Boore, 2010).

The median peak response (50$^{th}$ percentile) or RotD50 spectra is the definition that had been use in all representations of the earthquake hazard until recently (Palma Parra and Kowalsky, 2023; Stewart et al., 2011). The incorporation of RotD100 spectra into the building design code, specifically ASCE 7 (ASCE/SEI, 2010), raised concerns and highlighted the need to evaluate its potential implications in seismic structural design. Figure 3 shows displacement spectra defined for each component, RotD50 and RotD100 for a ground motion pair. This figure illustrates how for the same limit state displacement differing spectra definitions (RotD50 vs RotD100) can lead to different effective periods ($T_{50} > T_{100}$) and consequently different stiffnesses and strengths ($K_{50} < K_{100} \therefore V_{50} < V_{100}$). As stated previously, the DDBD approach employs displacement

spectra directly in its procedure and as it can be observed in Figure 3, the choice of RotDnn will impact the calculated effective period.

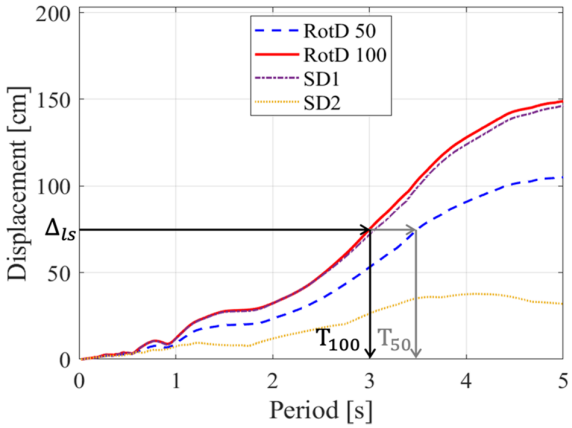


*Figure 3. Comparison of demands from RotDnn spectra using displacement spectra for as-recorded ground motion pair from the 1992 Landers earthquake.*

The literature has focused on the relationship of the median, 50$^{th}$ percentile, to RotD100, mainly to be able to convert the RotD50 design spectra to RotD100 design spectra. Shahi and Baker (2014) conducted a study for a subset of the NGA-West 2 database using 15,750 recordings from 326 earthquakes from shallow crustal active regions and found a conversion ratio for RotD50 to RotD100 response ($Sa_{RotD100}/Sa_{RotD50}$). Figure 4 shows the geometric mean of the spectral accelerations from their study with an average of 1.2 and a variation of ~8% as a function of period. Figure 4 also shows the inverse of this ratio, showing that, for this large dataset, RotD50 response is on average 80% of the RotD100 response.

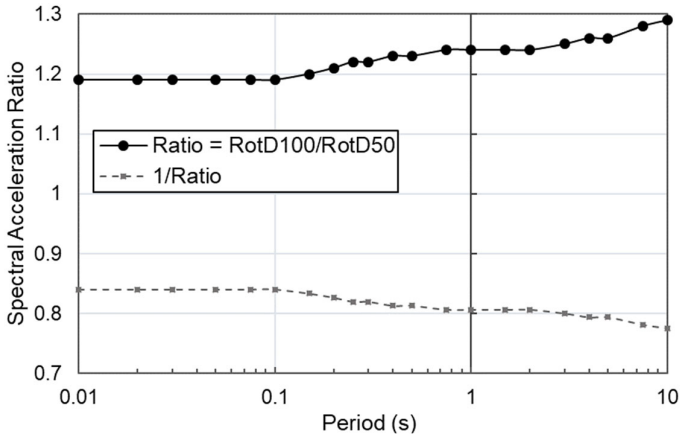


*Figure 4. Ratio of spectral accelerations between RotD100 and RotD50 from Shahi and Baker (2014).*

In a recent paper, Palma Parra and Kowalsky (2023) evaluated the impact of the choice of percentile of peak response, whether RotD50 or RotD100, on the bidirectional structural response of azimuth-independent systems, using response spectra computed at different damping ratios, for the design of structures expected to reach different levels of ductility. Their findings are shown in terms of the ratio of maximum radial displacement ($\Delta_{max}$) from nonlinear time history analysis to expected target displacement ($\Delta_T$) from DDBD in Figure 5. Their findings indicate that choice of percentile of peak response ($nn$) matters for the estimation of the inelastic displacement demands because displacements exceed the expected response on average by 18% to 57% depending on the structure's period, coupling of response, displacement ductility capacity, and ground motion signal tectonic regime (Palma Parra and Kowalsky, 2023). They proposed displacement demand factors based on these findings for use in design and analysis methods that employ response spectra, such as DDBD or the displacement calculation methods in the AASHTO Seismic Guide Specifications (SGS) for Seismic Design (AASHTO, 2023). As shown in Figure 5, these factors are in terms of geometric mean of

the displacement ratios for columns designed to RotD50 and RotD100 spectra ($GM_{50}\ and\ GM_{100}$) and the 84th percentile of the displacement ratios ($GM_{nn}\ + 1\sigma$). Most notable for this paper, Palma Parra and Kowalsky (2023) demonstrate that the DDBD approach is suitable for design of azimuth-independent systems under bidirectional loading because the maximum inelastic responses for RC circular columns are closer to the RotD100 expected target response.

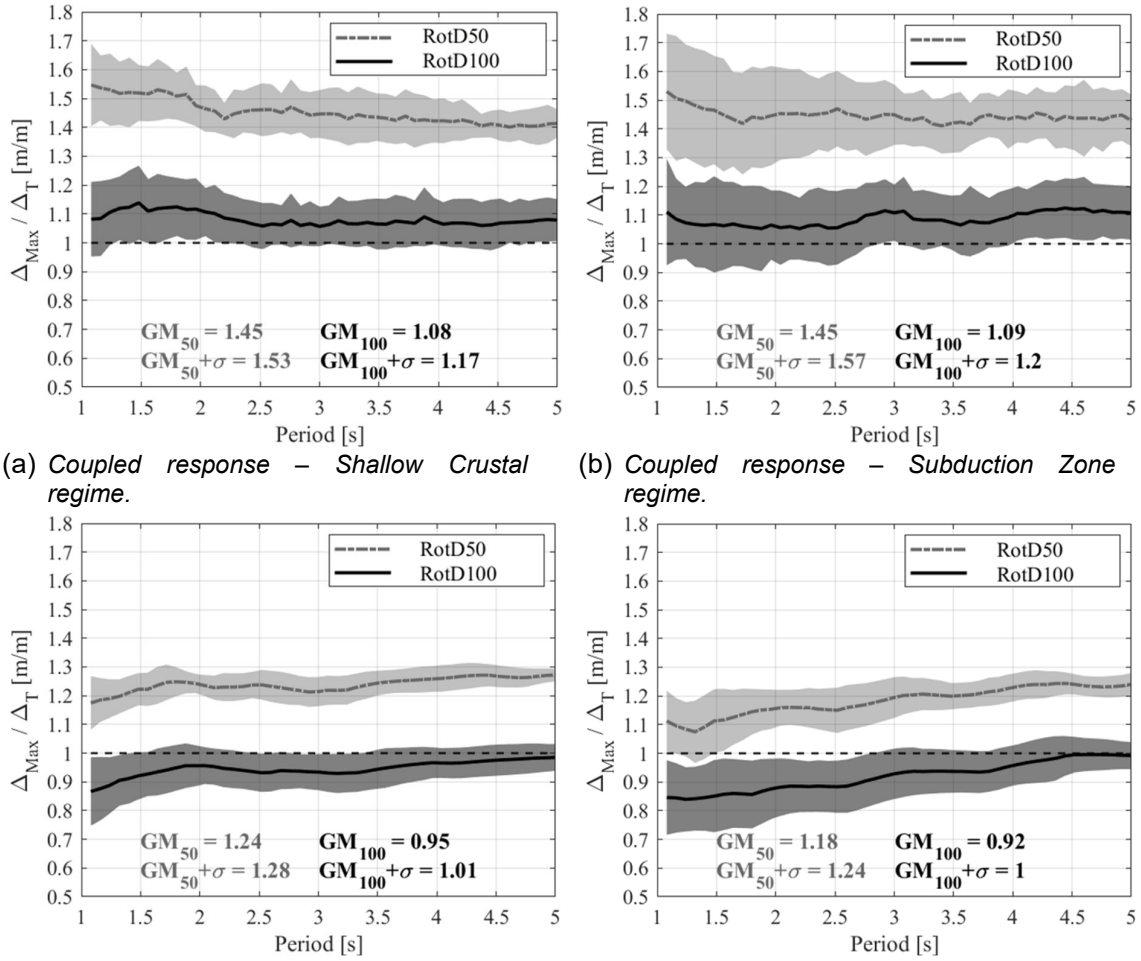


(a) *Coupled response – Shallow Crustal regime.*

(b) *Coupled response – Subduction Zone regime.*

(c) *Uncoupled response – Shallow Crustal regime.*

(d) *Uncoupled response – Subduction Zone regime.*

*Figure 5. Displacement ratios (NTHA maximum displacement to Design target displacement) for RotD50 and RotD100 definitions for the two earthquake regimes across seven ductility levels. Mean and coefficient of variation across periods for the 21,000 RC columns designed to each spectra definition for each regime.*

Given the large impact that the choice of percentile (50th or 100th) on seismic design and response demonstrated by Palma Parra and Kowalsky (2023), the DDBD approach is well suited to account for this. For this reason, the relationships of eight percentiles (00th, 25th, 50th, 60th, 70th, 75th, 85th, and 90th) to the maximum ($nn^{th}/100^{th}$), RotD100 were quantified. A sample of 20 ground motion pairs from the Pacific Earthquake Engineering Research (PEER) Center was used to evaluate these relationships, with 10 from NGA-West 2 and 10 from NGA-Sub databases (Bozorgnia et al., 2014; Bozorgnia et al., 2021). Similar to the inverse ratio from Figure 4, the outcomes of this study are presented in terms of the mean inverse ratio of the spectral displacements to the maximum displacement from RotD100 spectra ($\Delta_{100}$) across a period range of 1 to 10 seconds in Figure 6. This mean inverse ratio is referred here forth as $Z_{nn}$ and is calculated following Equation 2, where $\Delta_{nn}$ is the spectral displacement at each of the eight percentiles ($nn^{th}$) and $\Delta_{100}$ is the spectral displacement at RotD100. Spectra were also damped at seven damping ratios ranging from 5% to 18%, however, no significant variation in these relationships was found due to damping ratio. Similarly, tectonic setting did not influence the values of $Z_{nn}$.

$$Z_{nn} = geomean\left(\frac{\Delta_{nn}}{\Delta_{100}}\right) \quad (2)$$

Figure 6a summarizes these observations showing the $Z_{nn}$ mean values at each percentile with its corresponding variation band ($\pm 1\sigma$). The value for the 50th percentile agrees with the literature in mean and variation band, which is significant given the much smaller number of ground motions considered in the present study. The $Z_{nn}$ ratios are recommended as spectra conversion factors from RotD100 to other percentiles of the peak response. Regarding application, the $Z_{nn}$ ratios can be used to simplify the DDBD approach. If the displacement spectrum is linear, $Z_{nn}$ can be used to relate the strength required at different percentiles relative to the strength required when using RotD100 spectrum in the DDBD approach (See Equation 3). Furthermore, the relationship between base shear at any percentile and the base shear for RotD100 shows that the DDBD strength ratio ($V_{nn}$) for any percentile to the maximum is directly proportional to the square of $Z_{nn}$, as demonstrated in Equation 4. In this manner, when the DDBD method is used to design to RotD100 spectra, the $V_{nn}$ can be used to compute the strength at any other percentile of the spectra. Figure 6b shows $V_{nn}$ as the fraction of the maximum base shear force, along with the 1-standard deviation band ($\pm 1\sigma$). Note that these $V_{nn}$ factors are primarily suitable for use with linear spectra because they are based on averages across all periods. As part of the Ph.D. studies of the second author, recommendations for values of $nn$ are currently under development for various bridge systems. This will be accomplished by a statistical evaluation of the bi-directional response of bridges under rotating input motions. Once these recommendations are finalized, the application of the DDBD approach for designing bridge systems while accounting for directionality will be straightforward and will incorporate the outcomes presented in Figure 6.

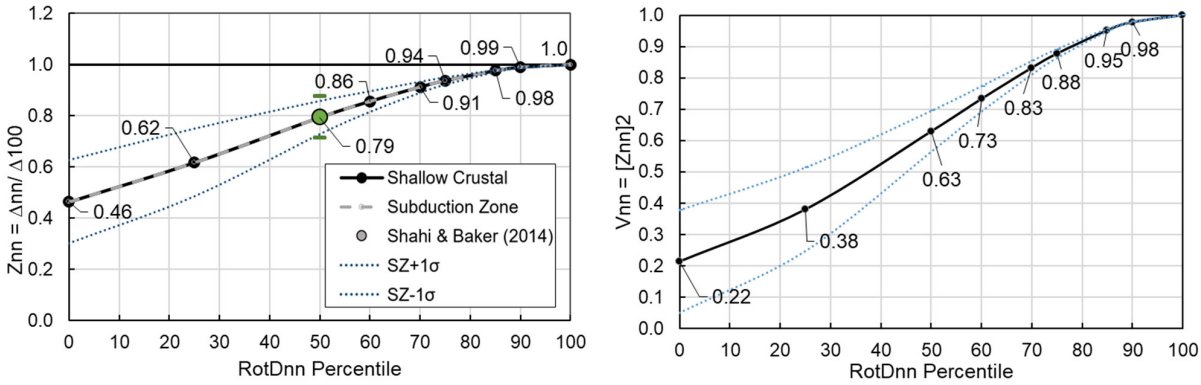


(a) $Z_{nn}$ *ratio compared to Shahi and Baker (2014)* (b) $V_{nn}$ *ratio*

*Figure 6. Mean $Z_{nn}$ and $V_{nn}$ ratio for the eight RotDnn percentiles with their corresponding variation and compared to Shahi and Baker (2014) value at 50th percentile.*

$$V_{B_{nn}} = V_{B_{RotD100}}(Z_{nn})^2 \quad (3)$$

$$V_{nn} \propto (Z_{nn})^2 \quad (4)$$

## 3. Simplification of the DDBD Approach – Equivalent Viscous Damping

The simplification of the DDBD approach for SDOF and MDOF systems can take many paths. In this section, we refer to the simplification related to the calculation of damping. While the DDBD procedure is conceptually simple, there are potential areas of simplification that could facilitate further implementation. One such area of simplification proposed here is the calculation of equivalent viscous damping. The fundamentals of the DDBD approach are summarized in Figure 7 (Priestley et al., 2007). Consider Figure 7c, which represents the relationship between damping ($\xi$) and displacement ductility ($\mu_\Delta$) for different structural systems characterised by different hysteretic rules. For example, concrete frame buildings would use the 'Takeda Fat' (TF) relationship while bridge columns would use the 'Takeda Thin' (TT) relationship.

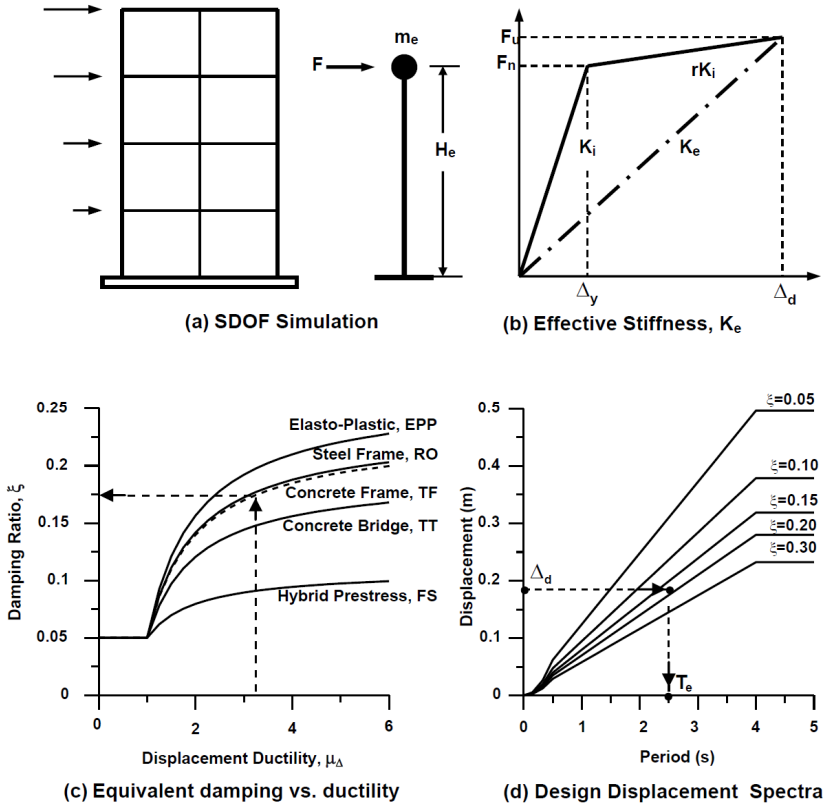


*Figure 7. Overview of fundamentals of Direct Displacement-Based Design (Priestley et al., 2007).*

As is evident from Figure 7c, while there is variation in damping at low ductility levels, at higher levels of ductility, damping is more stable. It is interesting to investigate the implication of this observation on the required base shear capacity. The values of damping are shown in Table 1 and plotted in Figure 8a for the different hysteretic systems. Numerically, the RO relationship can be excluded from this table since it is very similar to the TF relationship at four levels of displacement ductility. With reference to Equation 1, if the target displacement, hazard, and geometry remain the same, the base shear varies only in proportion to the damping as shown in Equation 5.

*Table 1. Damping ductility relationships for the hysteretic systems including Flag Shape (FS), Takeda Thin (TT), Takeda Fat (TF), and Elasto-Plastic (EPP).*

| $\xi$ (%) | FS | TT | TF | EPP |
|---|---|---|---|---|
| $\mu_\Delta = 2$ | 8.0 | 12.0 | 14.0 | 15.7 |
| $\mu_\Delta = 4$ | 9.4 | 15.6 | 18.5 | 21.0 |
| $\mu_\Delta = 6$ | 9.9 | 16.7 | 20.0 | 22.8 |
| $\mu_\Delta = 8$ | 10.2 | 17.4 | 20.7 | 23.7 |

$$V_b \propto \frac{7}{2+\xi} \tag{5}$$

The values of base shear are shown in Figure 8b, normalized to the values of the ‘Takeda Thin’ response. Note that values of base shear are minimally impacted by ductility for a given hysteretic response when normalized to Takeda Thin. Similarly, the design base shear can be calculated as a function of displacement ductility. Referring to Equation 1, if only ductility varies, then the design displacement and damping ratio will vary, resulting in Equation 6. Base shear values can be determined relative to the values at ductility 4 for all

hysteretic systems, as shown in Figure 8c. It is notable that the base shear value at a specific ductility level relative to the reference ductility of 4 appears to be insensitive to the type of hysteretic system.

$$V_b \propto \frac{1}{\mu} \cdot \frac{7}{2+\xi} \tag{6}$$

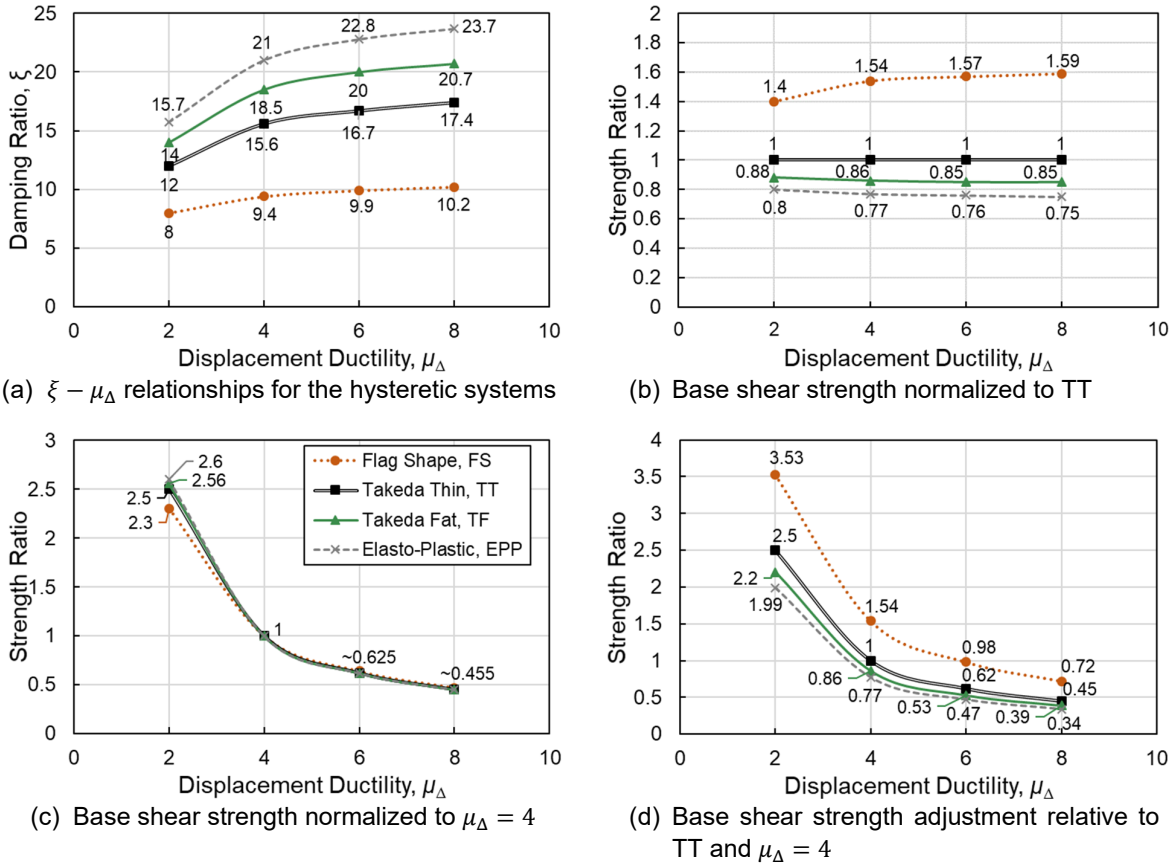


(a) $\xi - \mu_\Delta$ relationships for the hysteretic systems

(b) Base shear strength normalized to TT

(c) Base shear strength normalized to $\mu_\Delta = 4$

(d) Base shear strength adjustment relative to TT and $\mu_\Delta = 4$

*Figure 8. Simplification of damping calculation for different hysteretic structural systems.*

Combining the observations from Figure 8b and Figure 8c, a 'baseline strength' can be defined for all structures equal to that obtained from Takeda Thin at a displacement ductility of 4. This baseline strength ratio is shown in Figure 8d. Recalling Equation 1, this simplifies the design base shear to Equation 7, which is a function of only the system yield displacement, effective mass, and design response spectra. The resulting strength can then be adjusted based on Figure 8d to determine the required strength for different hysteretic systems and different ductility levels. Equation 7 assumes inelastic response greater than or equal to ductility 2. It should be noted that for elastic response, the required strength is the same for all hysteretic systems.

$$V_b \propto \frac{4\, m_e}{\Delta_y} \cdot \frac{\Delta_c^2}{T_c^2} \tag{7}$$

For SDOF systems, this simplifies the approach. For example, consider a two-span bridge with abutments free to translate and the pier consisting of a column 8m tall and 1.5m diameter. The yield displacement can be estimated with Equation 8 as $\Delta_y = 65mm$. If the column supports an inertia mass of 500,000kg, and the seismic demand is defined by a corner point displacement ($\Delta_c$) of 1m and a corner point period ($T_c$) of 4 seconds; the base shear is 1920kN (from Equation 7), which as noted before assumes a target displacement consistent with $\mu_\Delta = 4$. If the target displacement is instead consistent with a $\mu_\Delta = 8$ the design base shear is reduced to 45% of 1920kN (see Figure 8d), which would result in a base shear of 864kN.

In the case of a multi-storey building, the process would be as follows. The effective mass is estimated as 70% of the entire building weight. The yield displacement, determined at the effective height (calculated as 70% of

the total building height), can be found using Equation 9 for concrete moment frames, Equation 10 for steel moment frames, or Equation 11 in the case of structural wall buildings. Following this, Equation 7 is applied and the resulting base shear is adjusted according to Figure 8d. This approach was applied to the example multi-storey frame illustrated in Figure 9.

$$\Delta_y = \frac{\phi_y (H + L_{SP})^2}{3} \; or \; \frac{\phi_y (H + L_{SP})^2}{6} \tag{8}$$

$$\Delta_y = \theta_y \cdot H_e \quad where \; \theta_y = 0.5\varepsilon_y \cdot \frac{L_b}{h_b} \tag{9}$$

$$\Delta_y = \theta_y \cdot H_e \quad where \; \theta_y = 0.65\varepsilon_y \cdot \frac{L_b}{h_b} \tag{10}$$

$$\Delta_{yi} = \frac{\varepsilon_y}{l_w} \cdot H_i^2 \left(1 - \frac{H_i}{3H_n}\right) \tag{11}$$

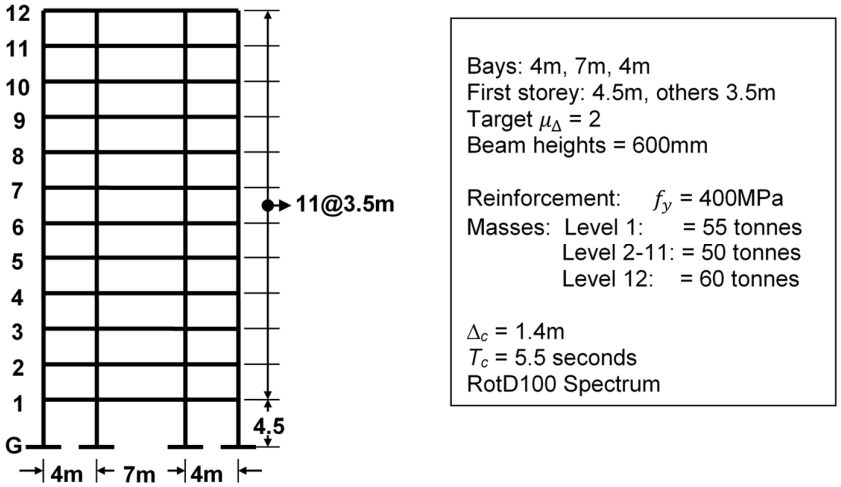


*Figure 9. Sample Multi-story frame design.*

From Equation 9, the yield rotation for the 4m bays equals $\theta_y = 0.00667$, while the yield rotation for the 7m long bay equals $\theta_y = 0.01167$. The average storey yield rotation can be estimated as $(2 \times 0.00667 + 0.01167)/3 = 0.00833$. Multiplying this by 70% of the building height results in a yield displacement of $0.7 \times 43m \times 0.00833 = 251mm$. The effective mass assigned to the frame equals $0.7 \times (55 + 10 \times 50 + 60) = 430.5 \; tonnes$. From Equation 7, the normalized base shear ($\mu_\Delta = 4$, Takeda Thin) equals 445kN. This serves as a baseline design that can be easily adjusted for different structural systems and limit states. Following Figure 8d, multiplying the normalized base shear by 2.2 (from Takeda Fat and a ductility of 2 in Figure 8d) results in a design base shear of 978kN. Full application of the DDBD approach to this same structure results in a required strength of 1024kN, which is within 5% of the value from the simplified method. This example is only illustrative, however it shows the potential simplicity that can be achieved by deploying a normalized base shear and effective height and mass factors of 0.7.

This example can also be used to demonstrate the simplification of DDBD to account for ground motion directionality, as described in Section 2. As noted in Figure 9, this multi-storey building was designed using a RotD100 spectrum. If instead, another percentile of the response was desired, say 60th or a RotD60 spectrum, then the design base shear obtained from the simplified damping DDBD approach can be modified by the respective $V_{nn}$ ratio, as shown in Figure 6b, which would lead to a lower design strength of $978 \; kN \times 0.73 = 714 \; kN$.

## 4. Other Challenges

The DDBD approach has been shown to be accurate at controlling structural performance for a variety of systems (Priestley et al., 2007); however, there are additional complexities that could be addressed in future simplifications. In the case of bridge structures, this includes the a priori definition of the displaced shape, changes of the design spectral shape, and ground motion directionality effects on bridge design.

### 4.1. **Displaced shape**

Computation of the displaced shape of a multi-span bridge under transverse loading is currently an iterative procedure in the DDBD approach as illustrated in Figure 9. The approach starts by assuming an initial shape and estimate of the proportion of force (x) carried by abutments and columns. Simplification of the transverse displaced shape consists of characterizing an initial shape with an educated guess that minimally influences the outcome. The typical displaced profile of a building is based on past studies where a large number of NTHA were conducted. A similar systematic analysis has yet to be done for bridges. For example, consider the 4 different bridges shown in Figure 2. This set of bridges have different column height configurations leading to different degrees of irregularity. The NTHA results for all four bridges show displaced shapes that are similar to each other. Conducting a systematic evaluation of displaced shape obtained from NTHA for different bridge geometries can provide insight to define a design target displaced shape based on bridge configurations, removing (or reducing) the need for iterations in the DDBD procedure for bridges. In this manner, a target displaced shape would be assumed from the start for with a high level of confidence for common bridge configurations. This shape could then be slightly adjusted depending on degree of irregularity and could be a function of differences in column heights, span lengths, or abutment conditions. One of the objectives of the second author's Ph.D. studies is to provide the necessary data to support this simplification.

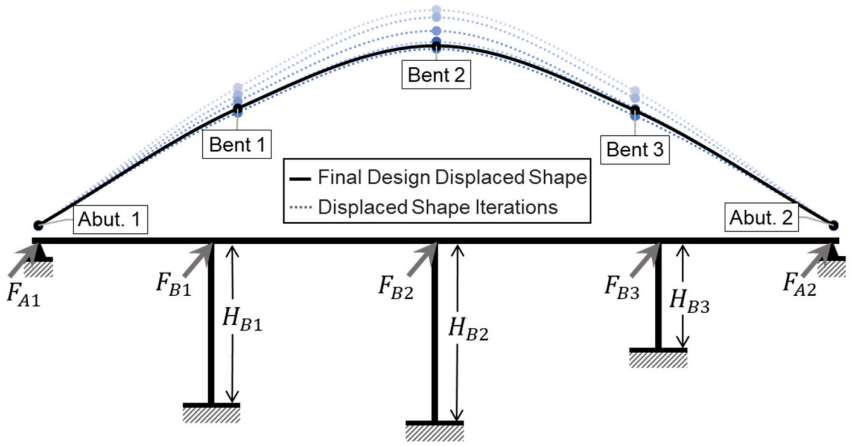


*Figure 9. Schematic of transverse displaced shape convergence in the DDBD approach.*

### 4.2. **Spectral Shape: 2-point versus Multi-point Spectra**

Response spectra provided by both the AASHTO LRFD Design Specifications (2014) and AASHTO Guide Specifications for LRFD Bridge Design (2016 edition) define spectral ordinates at two different periods for a return period of 975 years and are adjusted based on local site conditions using established factors. The latest update of the USGS uniform hazard model in 2018 introduced 22 spectral ordinates at discrete periods up to 10 seconds in the response spectra curve (BSSC, 2020) and has been incorporated into the 2023 edition of the AASTHO SGS. A comparison of the 2-point versus the new 22-point design spectrum for Charleston, SC is shown in Figure 10.

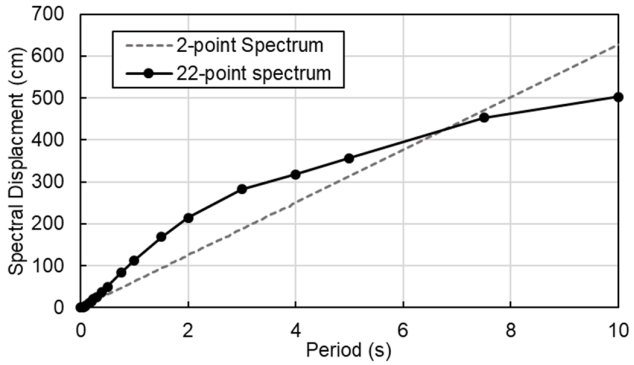


*Figure 10. 2-point spectrum versus 22-point spectrum for Charleston, SC.*

The adoption of smooth spectral shapes must be addressed in order to retain a simple base shear equation for DDBD (see Equation 1). As shown in Figure 10, a corner displacement ($\Delta_c$) and corresponding period ($T_c$) are not easily determined from the multi-point spectrum, which means Equation 1 cannot be used in this case. To address this issue, one can take different approaches. One would be to use conservative assumed values for $T_c$ and $\Delta_c$, by employing a tangential linear approximation of the 22-point spectrum. Alternatively, one can conduct the DDBD approach using the actual design DRS and interpolate between its discrete values. With respect to how this new spectral shape affects the directionality simplification in DDBD, before applying the $V_{nn}$ ratios (introduced in Section 2), these relationships should be explored to recommend factors for the 22-point spectra, considering that the slope can vary between discrete periods in both magnitude and direction.

### 4.3. **Ground Motion Directionality**

As of now, while the research community has continued to advance knowledge in this topic, there remains a lack of awareness regarding the definition of ground motion directionality in response spectra. As recognized by Stewart et al. (2011), Palma Parra and Kowalsky (2023), and others, there is still a need to understand how ground motion directionality affects the design of azimuth-dependent structures such as multi-span bridges, which have a preferred direction of response and different dynamic properties depending on direction. Underestimation of displacement demands by as much as 65% as shown in Figure 5 for RC columns (Palma Parra and Kowalsky, 2023) is unacceptable in the context of performance-based seismic design, and such errors can occur if the definition of the hazard is not well understood. We recognize that the value of RotDnn for bridges may differ from the current definition, RotD50, used in design codes.

Furthermore, a clear understanding of the bidirectional behaviour of bridges under bidirectional simultaneous input is important. From literature on the bidirectional response of RC columns, the combined action from bidirectional lateral loading has been shown to lead to reductions in the strength, displacement capacity, and ductility in comparison to its unidirectional response (Kawashima et al, 2003; Rodrigues et al., 2013). In addition, due to the coupling effect, strength and stiffness degradation occur in the column's biaxial hysteresis leading to larger energy dissipation (Wong et al., 1993; Kitajima et al., 1996; Chang, 2010; Arias-Acosta and Sanders, 2012). In contrast, since bridges are azimuth-dependent systems, the variation in their behaviour under bidirectional loading is expected to have larger differences depending on orientation of demands and biaxial interaction. Figure 11 illustrates the potential range of a bridge response, in terms of transverse displacements, as a function of the rotation of bidirectional seismic loading. This behaviour should be understood in conjunction with the appropriate definition of the bidirectional spectra (RotDnn) to be able to provide informed design recommendations.

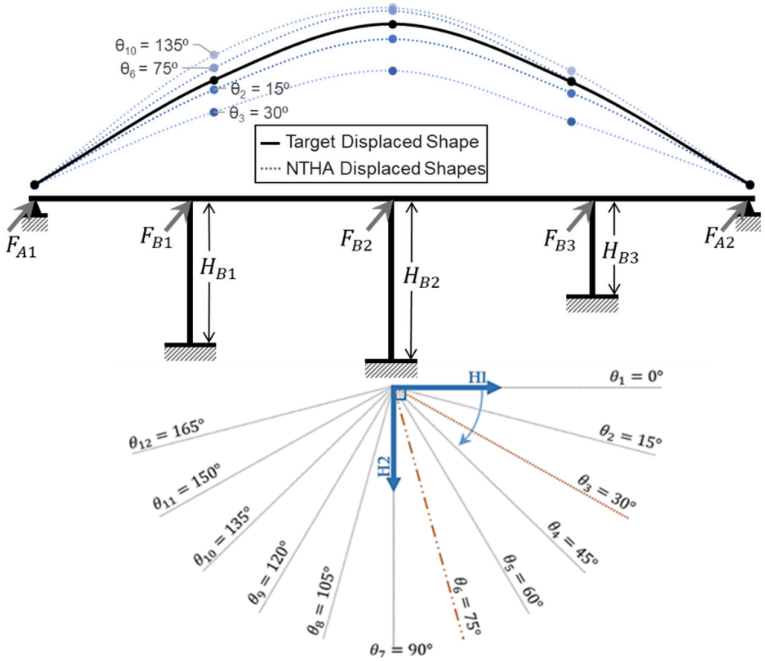


*Figure 11. Schematic of bridge subjected to ground motion pairs at Δθ=15° from 0° to 180°.*

## 5. Concluding Remarks

In this paper, we examine the past, present, and future of the Direct Displacement-Based approach, which was first introduced by Priestley in 1993. From SDOF systems to more complex building and bridge systems, the methodology has grown, adapted, and been verified. The DDBD approach will be included in the AASHTO performance-based design guidelines as an alternative bridge design approach (AASHTO, 2023). Herein, we discussed two steps to facilitate the approach's implementation into practice by reducing the effort to define the equivalent viscous damping, and accounting for bidirectional ground motions. The damping simplification introduces the use of a baseline design, assuming a single target ductility and hysteretic response ($\mu_\Delta = 4$, Takeda Thin), that can be easily adjusted for different structural systems and limit states. To account for ground motion directionality, the simplification makes use of two new parameters. The $Z_{nn}$ ratios are recommended as spectra conversion factors from RotD100 to any other percentiles of the peak response while the $V_{nn}$ factors can be used to compute the system's required strength at any other percentile of the spectra using the RotD100 design as a baseline. Lastly, we discussed future simplifications related to target displaced shape, spectral shape, and directionality. It is the hope of the authors that development of these changes will lead to further adoption of the design method, which is well suited to performance-based seismic design.

## References

AASHTO (2014) AASHTO LRFD Bridge Design Specifications. Customary U.S. Units (Seventh Edition), with 2015 and 2016 Interim Revisions.

AASHTO (2023) AASHTO Guidelines for Performance-Based Seismic Design of Highway Bridges.

Arias Acosta JG and Sanders DH (2012) Evaluation of the seismic performance of circular and interlocking RC bridge columns under bidirectional shake table loading. Proceedings of the 15th World Conference on Earthquake Engineering, Lisboa, Portugal.

Building Seismic Safety Council (BSSC) (2020) NEHRP Recommended Seismic Provisions for New Buildings and Other Structures (FEMA P-2082). Federal Emergency Management Agency: Washington, D.C.

Boore DM (2010) Orientation-independent, nongeometric-mean measures of seismic intensity from two horizontal components of motion. Bulletin of the Seismological Society of America 100(4): 1830-1835.

Bozorgnia et al. (2014) NGA-West2 research project. Earthquake Spectra, 30(3):973-987.

Bozorgnia et al. (2021) NGA-Subduction Research Program. Earthquake Spectra, 38(2):783-798.

Chang SY (2010) Experimental studies of RC bridge columns under axial load plus biaxial bending. Journal of Structural Engineering, ASCE 136(1): 12-25. DOI: 10.1061/(ASCE)0733-9445(2010)136:1(12)

Dwairi H and Kowalsky MJ (2006) Implementation of Inelastic Displacement Patterns in Direct Displacement-Based Design of Continuous Bridge Structures. Earthquake Spectra, 22(3):631-662.

Kawashima K, Sasaki T, Kajiwara K, Ukon H, Sakai J, Takahashi Y, Kosa K, and Jabe M (2009) Seismic performance of RC bridge columns subjected to bilateral excitation. Invited paper for Structural Engineering/Earthquake Engineering, Japan Society of Civil Engineers, 6(1):28s-46s.

Kitajima K, Adachi H., Nakanishi M (1996) Response Analysis of RC columns under bidirectional earthquake motions. Proceedings of the Eleventh World Conference on Earthquake Engineering, Acapulco, Mexico.

Palma Parra AL and Kowalsky MJ (2023). Impact of Ground Motion Directionality (RotDnn) on the Coupled and Uncoupled Inelastic Response of RC Circular Columns. Earthquake Spectra 39(3): 1859-1882.

Priestley MJN, Calvi GM, and Kowalsky MJ (2007) Direct Displacement-Based Seismic Design of Structures. IUSS Press, Pavia Italy, ISBN 978-88-6198-000-6.

Priestley MJN (1993) Myths and Fallacies in Earthquake Engineering – Conflicts between design and reality. Proceedings of the Tom Paulay Symposium, San Diego.

Rodrigues H, Arede A, Varum H., and Costa AG (2013) Experimental evaluation of rectangular reinforced concrete column behaviour under biaxial cyclic loading. Earthquake Engineering and Structural Dynamics, 42: 239-259. DOI: 10.1002/eqe.2205

Shahi SK. and Baker JW (2014) NGA-West2 models for ground motion directionality. Earthquake Spectra 30(3): 1285-1300. DOI: 10.1193/040913EQS097M.

Stewart JP, Abrahamson NA, Atkinson, GM, Baker JK, Boore DM, Bozorgnia Y, Campbell KW, Comartin CD, Idriss IM, Mathew L, Mehrain M, Moehle JP, Naeim F and Sabol TA (2011) Representation of bidirectional ground motions for design spectra in building codes. Earthquake Spectra 27(3): 927-937.

Wong YL, Paulay T, and Priesley MJN (1993) Response of circular reinforced concrete columns to multidirectional seismic attack. ACI Structural Journal, 90(2): 180-191.